Journal of Power Sources 196 (2011) 9488–9499

Contents lists available at ScienceDirect

Journal of Power Sources

journal homepage: www.elsevier.com/locate/jpowsour

Automation infrastructure and operation control strategy in a stand-alone power system based on renewable energy sources

Chrysovalantou Ziogou[a], Dimitris Ipsakis[a], Costas Elmasides[b], Fotis Stergiopoulos[a,c], Simira Papadopoulou[a,c], Panos Seferlis[a,d], Spyros Voutetakis[a,*]

[a] Chemical Process Engineering Research Institute (C.P.E.R.I.), Centre for Research and Technology Hellas (CE.R.T.H.), P.O. Box 60361, 57001 Thermi-Thessaloniki, Greece
[b] Systems Sunlight S.A., Neo Olvio, 67200 Xanthi, Greece
[c] Department of Automation, Alexander Technological Educational Institute of Thessaloniki, P.O. Box 141, 54700, Sindos, Thessaloniki, Greece
[d] Department of Mechanical Engineering, Aristotle University of Thessaloniki, P.O. Box 484, 54124 Thessaloniki, Greece

ARTICLE INFO

Article history:
Received 19 January 2011
Received in revised form 21 April 2011
Accepted 10 July 2011
Available online 20 July 2011

Keywords:
Stand-alone power system
Renewable energy sources
Hydrogen production
Automatic control
Power management strategy
Fuel cell

ABSTRACT

The design of the automation system and the implemented operation control strategy in a stand-alone power system in Greece are fully analyzed in the present study. A photovoltaic array and three wind generators serve as the system main power sources and meet a predefined load demand. A lead-acid accumulator is used to compensate the inherent power fluctuations (excess or shortage) and to regulate the overall system operation, based on a developed power management strategy. Hydrogen is produced by using system excess power in a proton exchange membrane (PEM) electrolyzer and is further stored in pressurized cylinders for subsequent use in a PEM fuel cell in cases of power shortage. A diesel generator complements the integrated system and is employed only in emergency cases, such as subsystems failure. The performance of the automatic control system is evaluated through the real-time operation of the power system where data from the various subsystems are recorded and analyzed using a supervised data acquisition unit. Various network protocols were used to integrate the system devices into one central control system managing in this way to compensate for the differences between chemical and electrical subunits. One of the main advantages is the ability of process monitoring from distance where users can perform changes to system principal variables. Furthermore, the performance of the implemented power management strategy is evaluated through simulated scenarios by including a case study analysis on system abilities to meet higher than expected electrical load demands.

1. Introduction

Greenhouse gas emissions (mainly CO_2, NO_x and CH_4) are the main contributors to global warming and are also related to the excessive usage of fossil fuels that meet the world's energy demands, from simple daily domestic needs up to heavy industrial applications. In order to prevent the aggravation of detrimental effects, environmental friendly solutions have to be proposed and applied. These solutions should focus on the elimination, or at least minimization, of carbon based fuels and should develop a both efficient and cost-effective, application that could replace conventional power production processes.

Stand-alone power systems based on renewable energy sources (RES), could offer off-grid power supply for the electrification of remote areas that are not connected to the main grid, the powering of telecommunication stations and the desalination of water; processes that require significant amounts of energy. Such integrated systems usually comprise a power production unit based on RES, complemented by short- and long-term energy storage units.

The rate of development and application of stand-alone power systems has increased significantly over the past few years. Starting from simple applications back in the 1990s with the exploitation of solar systems [1,2], the research society has moved to more complicated systems with the introduction of short-term and long-term energy storage units [3–5] that aim to the efficient and cost-effective operation accounting also for the variations in regional weather data. The analysis of such complicated and demanding systems has sparked the interest of theoretical studies that focus on the integration of the various units through overall power management strategies [6–10]. Design analysis based on the economic evaluation of the involved subsystems has also been another research area that is constantly developing [11–13] and lies on the optimal selection of system sizes and configurations. However, real-time operation of stand-alone power systems as implemented by the automation infrastructure and its mathematical modeling background, has received limited attention in literature. Most studies

* Corresponding author. Tel.: +30 2310498317; fax: +30 2310498380.
E-mail address: paris@cperi.certh.gr (S. Voutetakis).

0378-7753/$ – see front matter © 2011 Published by Elsevier B.V.
doi:10.1016/j.jpowsour.2011.07.029

focused on the description of individual subsystems along with their electronic parts [14–18], while other studies that describe the stand-alone power system as an entity, failed to address the important details and features regarding unit integration, their auxiliaries section (converters, inverters, etc.) and their overall operation. One of the few concrete studies over this research area is found in [5], where a quite sufficient approach for the description of the converters used in stand-alone power systems was presented, along with a brief analysis on their capacity and ability to deliver the amount of energy needed. Roncero-Sánchez et al. [19] also described the use of *PWM* (pulse-width modulation) converters for the connection of wind generators to the main grid. The characteristics of the electronic parts gave rise to the design of state-feedback controllers that can be used for current control. Despite the importance of system integration under well-designed converters, one of the vital parts for a reliable system operation is the data acquisition system. Agbossou et al. [20] and Little et al. [21] presented the architecture of an automatic operation that has been applied in two similar hydrogen-based systems utilizing solar and wind energy. All necessary connections were sufficiently described in conjunction with the monitoring system, but the applied power management strategy was limited shown. Koutroulis and Kalaitzakis [22] developed an integrated computer-based data-acquisition system for RES plants and the proposed method was based on an easy-to-use graphical environment, for processing, displaying and storing the collected data. In their study, they proposed the remote-user operation that is essential in autonomous applications.

The aim of this paper is to present a complete study that focuses on the automation system design and its implementation in a stand-alone power system located at Neo-Olvio, Xanthi, Greece [6]. The main challenge in such complicated systems is the successful integration of the involved units. All different devices are integrated into one central control unit and based on their communication protocols an overall Supervisory Control and Data Acquisition System is developed. A user friendly-environment is also proposed in order to allow for remote operation and system monitoring. Along with the analysis of the control architecture and the integrated infrastructure an algorithm (power management strategy) has been developed for the efficient operation of the system. The algorithm performance is assessed through a simulated scenario at three different load demand levels. The objective of the theoretical simulation analysis is (i) to calculate the contribution of the subsystems towards a reliable system operation, (ii) to identify design modifications needed for the protection of the subsystems from excessive utilization that can limit their operating lifetime and (iii) to maintain the eco-friendly character of the application through the implementation of the control strategy. Such an analysis is considered as a necessary step prior to scale-up attempts and consistent with the operation planning of stand-alone power systems.

2. Description of the main units in the stand-alone power system

The stand-alone power system under consideration consists of several subsystems that contribute with different levels towards meeting a load demand. A photovoltaic system (*PV*) consisted of 144 photovoltaic panels, each one rated at 69.4 W_p results in a total installed capacity of 10 kW_p with an overall average efficiency of 10%. Three wind generators rated at 1 kW_p each, are also installed and contribute to the wind energy exploitation. The energy storage system comprises short-term and long-term storage units. The short-term power needs (in a time scale of minutes up to a few seconds) are satisfied through parallel strings of lead/acid cells of similar capacity, contributing to an overall accumulator of 3000 Ah (4×750 Ah). Each accumulator bank consists of 24 cells connected in series, with a nominal voltage of 2 V each, thus providing a nominal DC-bus voltage of 48 V. The accumulator is a critical element for the efficient operation of the autonomous energy supply system as it regulates the power flow in the system. The long-term power needs are met by a hydrogen-based system that is consisted of a PEM electrolyzer, a hydrogen storage unit and a PEM fuel cell. The PEM electrolyzer is supplied with pure water at the anode and through the utilization of electrical power, hydrogen is produced at the cathode. The minimum and maximum power levels that the electrolyzer is allowed to operate as set by the manufacturer are 1.05 kW ($P_{min,elec}$) and 4.2 kW ($P_{max,elec}$), corresponding to 25% and 100% of the nominal power, respectively. The produced hydrogen is initially stored in buffer tanks until the pressure inside these tanks reaches a preset limit of 7 barg. At that point, a hydrogen compressor raises the gas pressure to the final storage pressure levels ranging between 15 and 30 barg. In this way, the buffer tank serves as a regulatory unit to compensate for fluctuations in the hydrogen production rate and also allows for significant energy savings [6,7]. The capacity of the final hydrogen storage system is 1 m^3/at 30 bar which is equivalent to around 35 kWh. The stored hydrogen is utilized during periods of power deficit in the autonomous system in a PEM fuel cell, rated at 4 kW_p. Hydrogen is supplied at the anode whereas air is supplied at the cathode. The produced water is collected and stored in a tank to be subsequently utilized in the electrolyzer so that a self-sustain closed loop system in water is maintained. Strict water quality specifications apply and therefore a water monitoring and conditioning unit is installed. In case the stored hydrogen is not sufficient to meet the system power deficit, an installed diesel generator provides the necessary power to the system, but is mainly considered as a back-up emergency unit. The system components are connected through multiple relevant converters of each kind, DC/DC (PV array, fuel cell), AC/DC (wind generators, electrolyzer, diesel generator), to the accumulator which forms the DC bus. There the energy is either stored by the charging sources (fuel cell, diesel generator, PV array, wind generators) or consumed by supplying the internal (electrolyzer, auxiliary units) and external load. A schematic of the installed componets and their interconnections is shown in Fig. 1. Information on the flow of energy (both chemical and electrical) via the subsystems is also provided. At this point it is highlighted that the sizing of each subsystem was based on the approach of Zhou et al. [13] and for the short-term energy storage system (accumulator) a prerequisite that was applied referred to an overall autonomy of 1–1.5 days during the worst case scenario.

3. Integrated infrastructure and implementation of the control system

Designing flexible control architecture is one of the key factors to enable interoperability, extensibility and automated operation of an autonomous power system. Furthermore, there is a need to integrate different devices into one central control system. The choice of the communication protocol is dictated by each device manufacturer and as a result, various network protocols are implemented in the stand-alone power system at Neo Olvio. These devices use common or industrial communication protocols such as RS-232C, Ethernet or Controlled Area Network (CAN). Also in order to transmit data from the site to a central master control unit, which is a Supervisory Control And Data Acquisition (SCADA) system, a distributed Profibus network is used. The fuel cell, the electrolyzer and the DC/DC converter use CAN protocol to communicate with the SCADA system, whereas the DC/AC inverters use common serial protocols which are converted through a serial bridge server into TCP/IP (Transmission Control Program/Internet

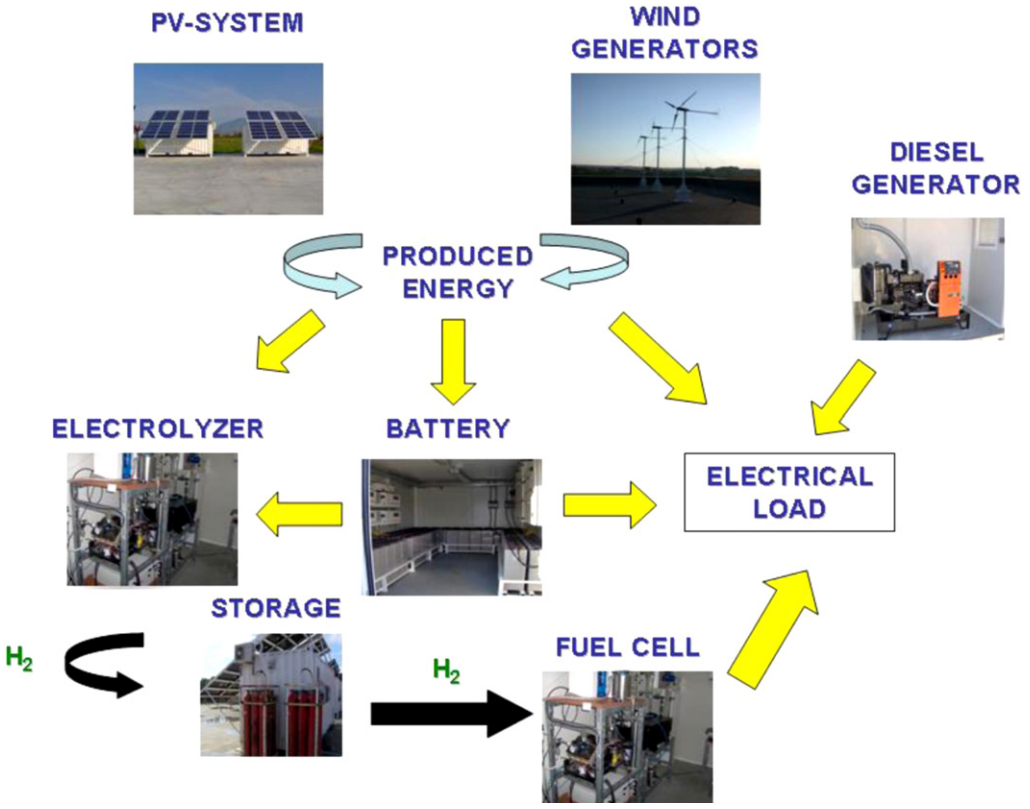

Fig. 1. Schematic of the stand-alone power system located at Neo Olvio, Xanthi, Greece.

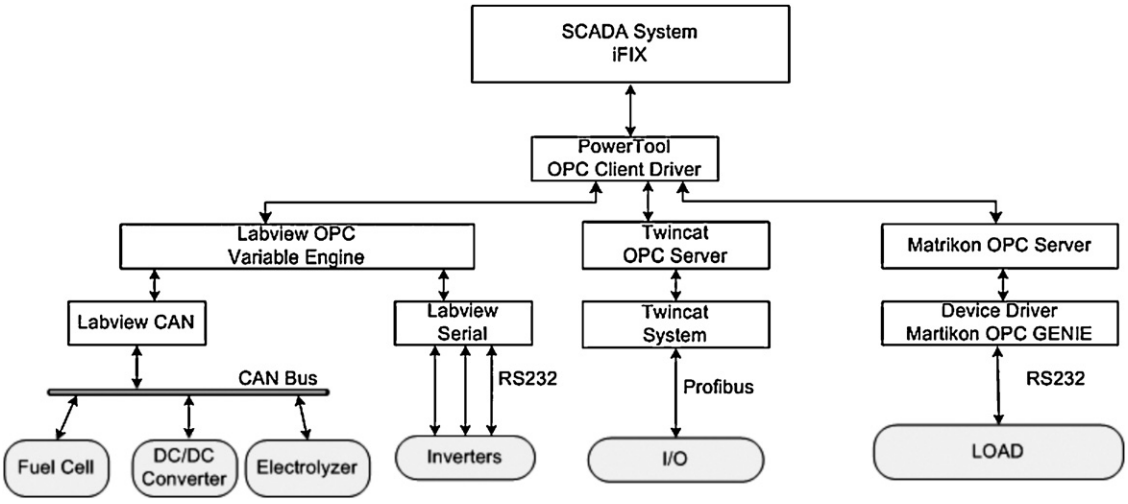

Fig. 2. Schematic representation of the automation system architecture.

Protocol) packets. All these different protocols are translated to an OPC (Ole Process Control)-based format due to homogeneity reasons. The implementation of such architecture creates a uniform centralized environment for the SCADA system, which is designed to collect and distribute system real-time data with flexibility and scalability. The schematic representation and the interconnection of the communication devices are presented in Fig. 2 [23].

One advantage of the stand-alone power system is the fact that its operation can be monitored remotely using standard browser-based technology. The user can make changes of key variables, such as the power supply level of the PEM electrolyzer or the current drawn from the PEM fuel cell, and monitor the system response. The data from the system operation are stored in an archiving system for easy retrieval by an authorized user and subsequent processing. Figs. 3 and 4 show screenshots of the graphical user interface of the integrated system in operation where real-time data are shown as graphical shapes over a static background. In Fig. 3 the overall electric energy flow is shown along with the interconnections of each subsystem to the main DC bus-bar. This primary interface shows a representation of the system in graphical form. On the left side of the interface the subsystems that produce power are shown (PV-array, wind generators (WG), diesel generator (BPU) and fuel cell), while on the right side the subsystems that require power (auxiliaries, load utilities and electrolyzer) are also monitored. In the middle part the accumulator (BAT) and the storage of hydrogen and water are presented. The flow diagram of the electrochemical

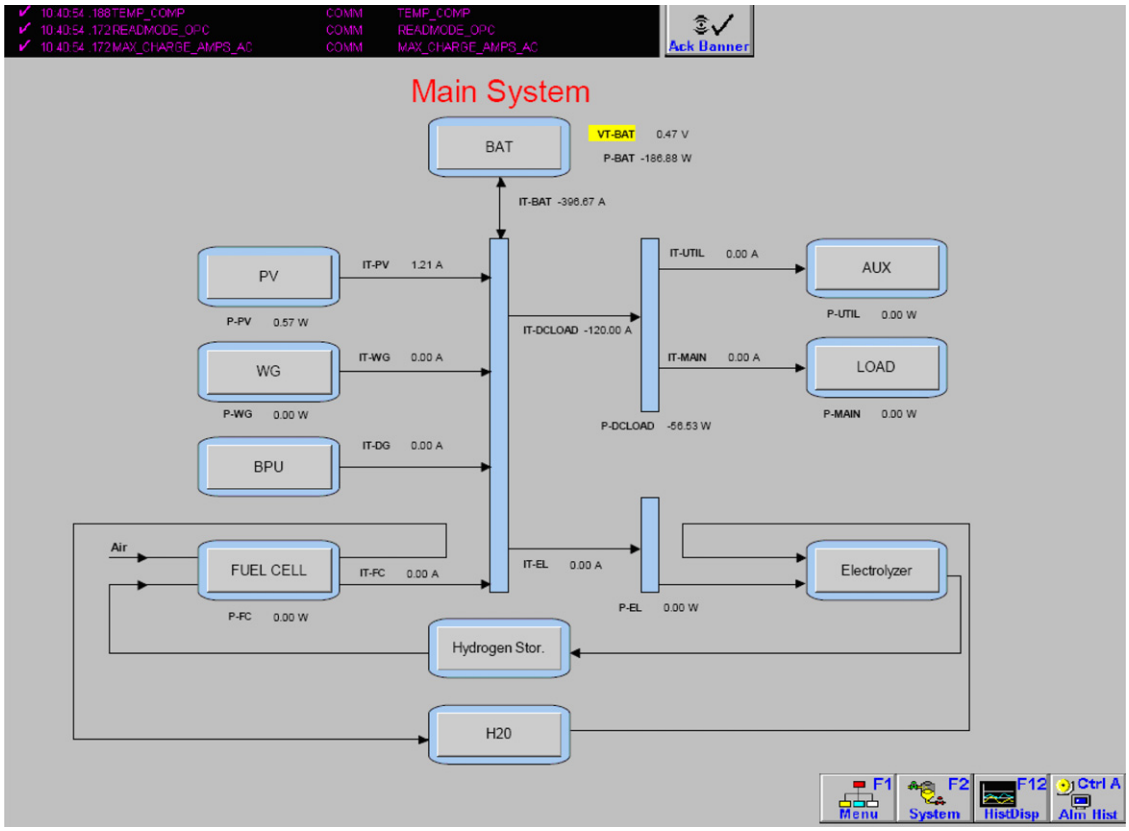

Fig. 3. SCADA system general layout (electrical system).

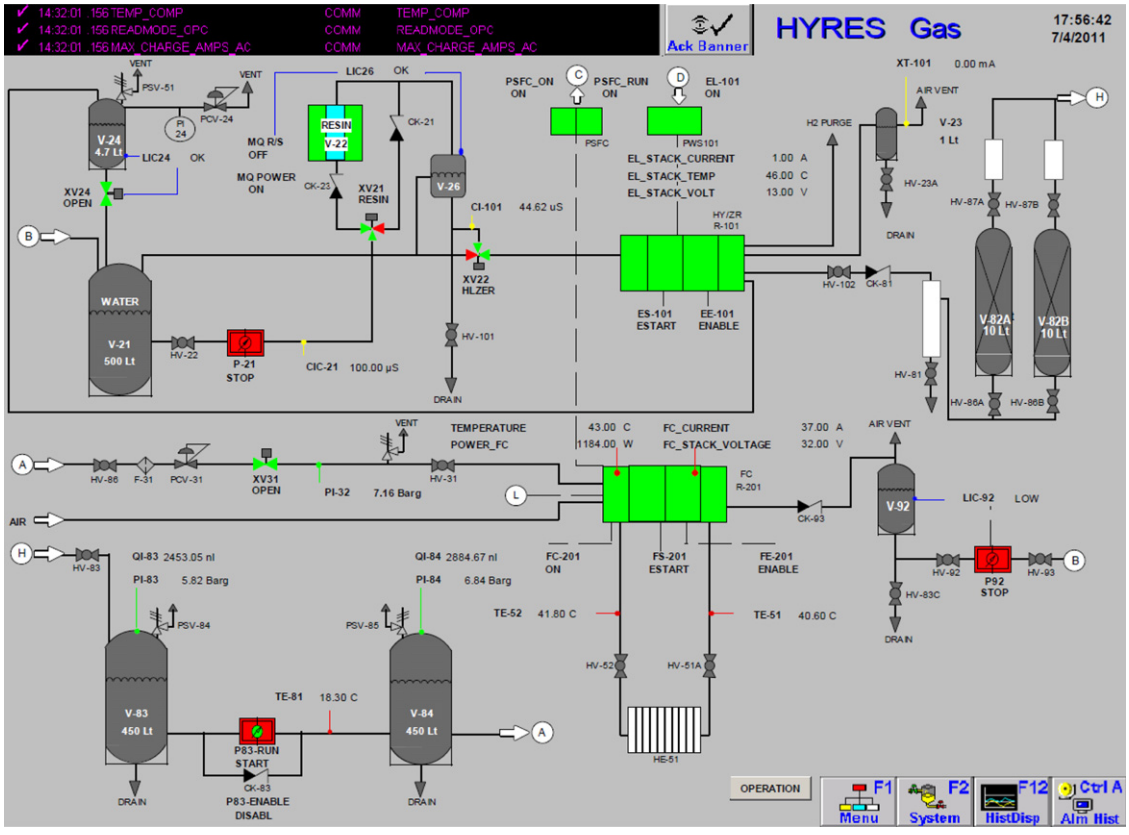

Fig. 4. SCADA system general layout (chemical system).

subsystem is presented in Fig. 4 and it consists of the electrolyzer (HY/ZR R-101), the compressor (P-83), the storage units (V-83 and V-84) and the fuel cell (FC R-201). Other subunits include water storage (V-21) and dehydrators (V-82). As can be seen, the fuel cell is in actual operation and 1.18 kW are being produced. The developed interface has an activated navigation and reporting features that enable the user to supervise the state of the overall system and decide for the subsystem operating pattern.

The utilization of the aforementioned architecture enables the study of the effects that the selected power management (or operation) strategy has to the system performance and also provides the ability to test and implement flexible automated algorithms of alternative strategies. The power management strategy relies on the estimation of the accumulator State-of-Charge (*SOC*). Thus, the *SOC* is the key system control variable that is maintained within specified upper and lower bounds. The *SOC* of the accumulator is calculated as:

$$SOC(t_2) = SOC(t_1) \cdot \sigma_{ac} + I_{ac} \cdot \eta_{ac} \cdot (t_2 - t_1) \quad (1)$$

where σ_{ac} is the self-discharging rate of the accumulator (%), η_{ac} is an efficiency factor with a value around 95%, I_{ac} is the operation current (A), and t_i is the time interval (h), for $i = 1, 2, \ldots, n$.

The *SOC* of the accumulator is a variable that can be estimated indirectly during the operation of the system, based mainly on voltage measurements [24–26]. Usually, specific accumulator experiments are performed and based on *I–V* measurements during charging and discharging cycles, an equation that relates the voltage with the accumulator's *SOC* can be derived and is unique for the type of the accumulator used. The desired accumulator *SOC* range for the reliable power flow in the system is easily related to voltage operating conditions. Operation within such a *SOC* range ensures that the accumulator can anticipate power fluctuations from the power generation units successfully. If *SOC* moves outside the desired range the system initiates the appropriate procedure in order to fulfill the electrical load demand. Therefore, the electrolyzer system is used when there is an excess of power and the *SOC* (or accumulator voltage) is above the maximum level, while in cases of power shortage, the system uses the stored hydrogen in order to meet the load demand through the operation of the fuel cell and *SOC* level is below a minimum value. Fig. 5 presents the flowchart of the implemented control algorithm [6].

Power deviations from the load demand are defined as (accordingly the energy deviations form the same equation with energy variable instead of power):

$$P = P_{RES} - P_{LOAD}, \quad (2)$$

where P is the power excess or shortage (W), P_{RES} is the power supply by the renewable energy sources (*PV* array and wind generators) (W) and P_{LOAD} is the load demand (W).

The power management strategy was developed based on the concept of Hierarchical Control Theory, which is mainly applied in electrical integrated systems and dictate the operation of the involved subsystems based on a predefined hierarchy made on the decision flow [27]. The basic steps presented in Fig. 5 are described in detail in Section 5.

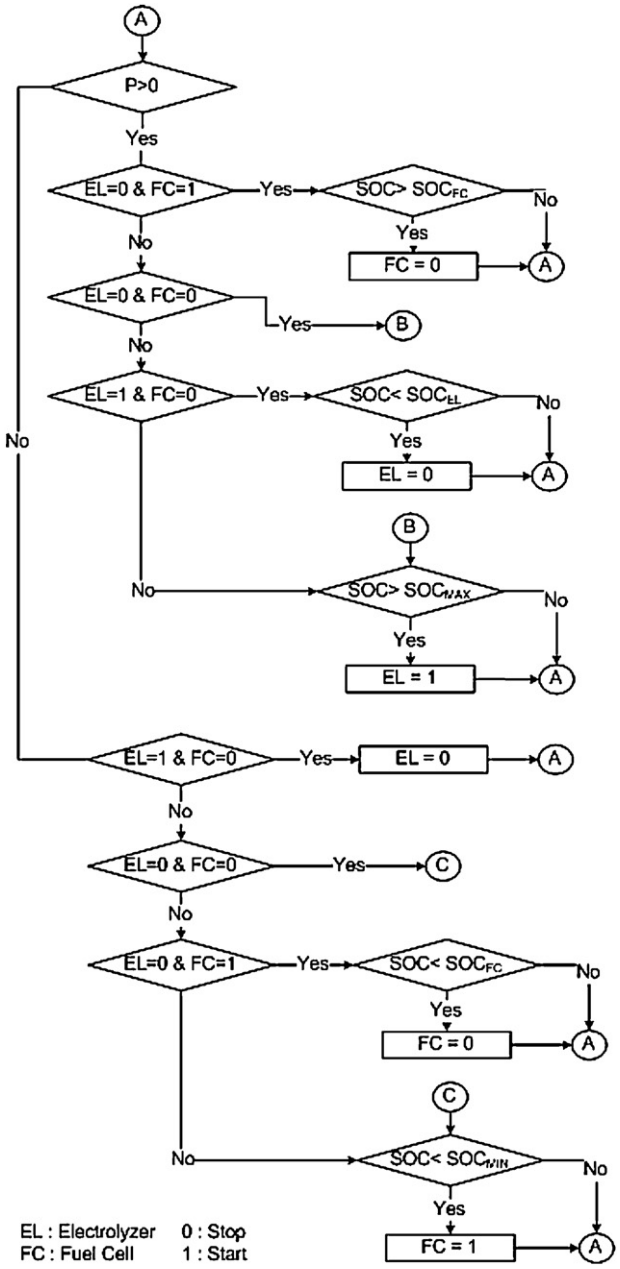

Fig. 5. Control algorithm flowchart of the autonomous operation.

4. Experimental results from the operation of the subsystems

In this section, the operating results for the main subsystems of the stand-alone power system are presented in order to evaluate their performance, as well as, the applicability of the automation architecture. All subsystems in the stand-alone power system are operating continuously and according to the operating policy depicted in Fig. 5. For the current study though, the main objective, as far as the sensitive subunits of the PEM electrolyzer and PEM fuel cell are of concern, is the evaluation of their start-up and shut-down dynamics and thus, these subsystems are tested separately (including the storage units) in the system with the help of an operator, either from a distance or on site. With such a dynamic testing, the performance of the installed power electronic converters can simultaneously be evaluated so as to minimize any potential faults.

4.1. Photovoltaic and wind generators systems

Fig. 6 shows the power output from the *PV*-system and the wind generators, as well as the utilities load power demand for a period of two-weeks in March 2011. The recorded maximum power levels are 7.1 kW_p for the *PV* system and 2.2 kW_p for the wind generators, whereas the minimum and maximum power levels are 0.5 and 2.2 kW_p for the load utilities, respectively. As it can be seen, the output power of the wind generators is rather low due to the

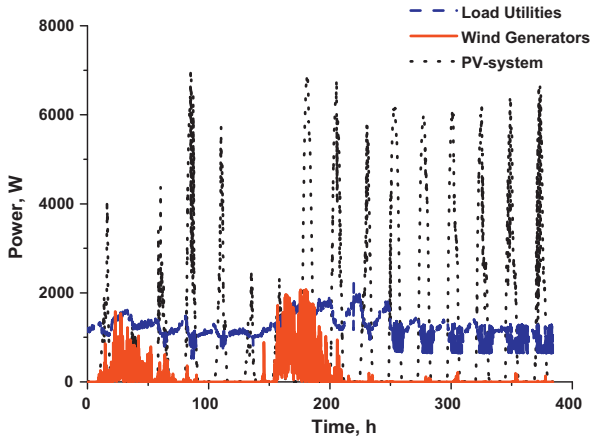

Fig. 6. Power levels of the *PV*-system, wind generators and load utilities over a period of two weeks.

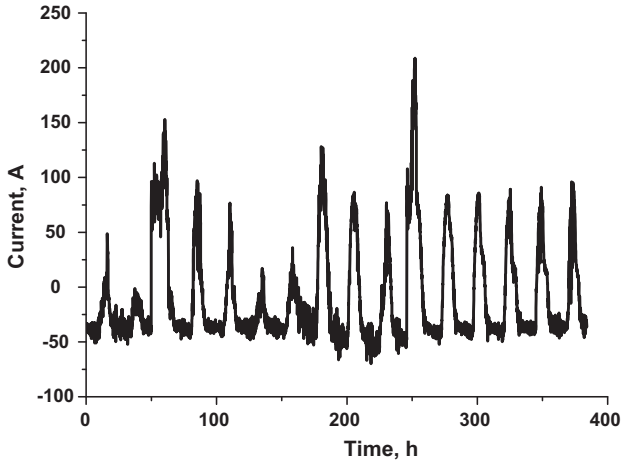

Fig. 7. Operating current of the lead-acid accumulator over a period of two weeks.

low local wind speeds at that time period, meaning that the load demand (utilities) was mainly met by the *PV*-system. In general, power deficit was exhibited in 71% of the time during the two weeks time period that was covered by the short-term storage unit of the accumulator that follows in the analysis.

4.2. Lead-acid accumulator

Fig. 7 shows the operating current of the lead-acid accumulator during the same time period. Negative values of current indicate discharging and positive values indicate charging of the accumulator. During this period time, when the *PV*-system provides enough power for the stand-alone power system to operate, excess power is available for charging the accumulator and consequently its operating voltage is increased (Fig. 8). After sunset, shortage of power usually exists and the accumulator is discharged to meet the system energy needs with a subsequent voltage reduction. An operation constraint that is imposed to the accumulator operation refers to the lower allowable limit of 48.2 V (corresponds to a *SOC* of 75–80%) that should not be surpassed. In such a case the diesel generator is connected to the DC-bus bar and sets to operation until the accumulator reaches a voltage level of 55 V. The inverter/charger scans the accumulator records and initiates the diesel operation. Fig. 8 shows the two time instances during the two-week time period that the accumulator reached its lower limits and forced the diesel generator to start operating (Fig. 9).

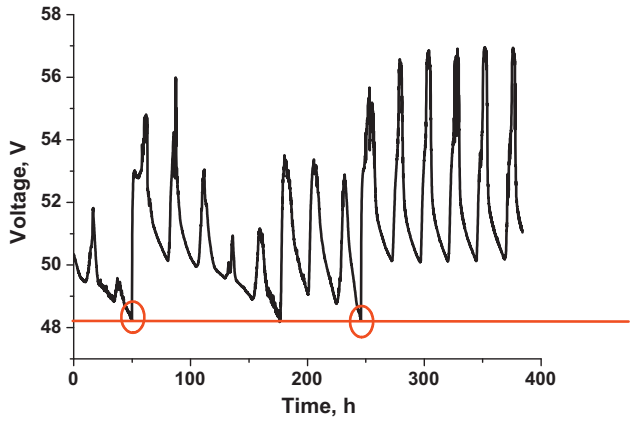

Fig. 8. Operating voltage of the lead-acid accumulator over a period of two weeks.

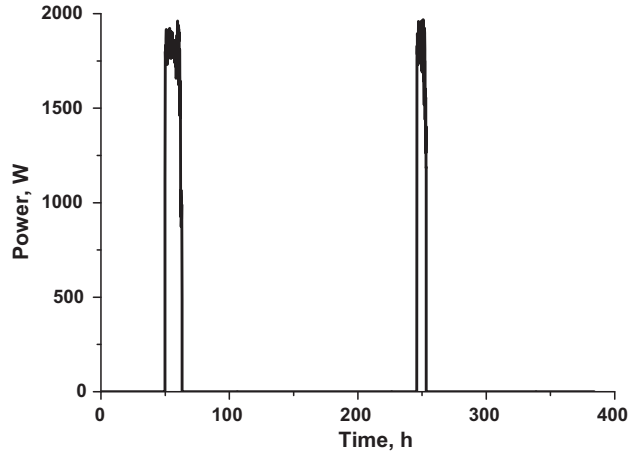

Fig. 9. Operating power of the diesel generator over a period of two weeks.

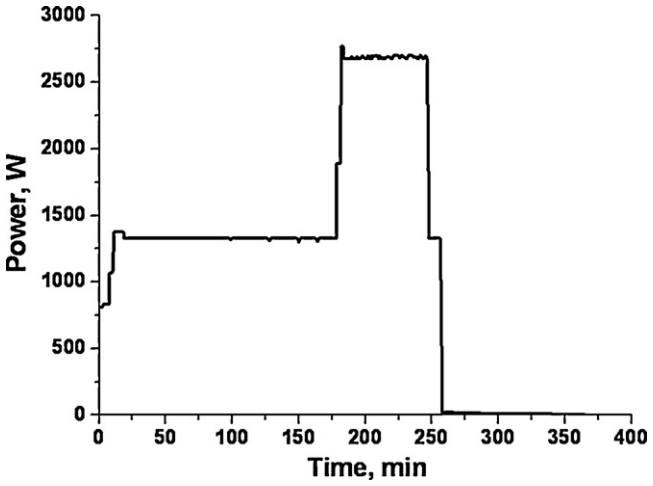

Fig. 10. Power level of the PEM electrolyzer operation.

4.3. PEM electrolyzer, PEM fuel cell and hydrogen storage unit

In a representative experiment, the operation of the electrolyzer was recorded and Fig. 10 shows the power levels during the time of operation. As it can be seen, the power levels of the electrolyzer are ranging satisfactory between the allowable limits of 1.05–4.2 kW. Only for a few minutes at the beginning of hydrogen production, the electrolyzer is recorded to operate at a lower level (around the

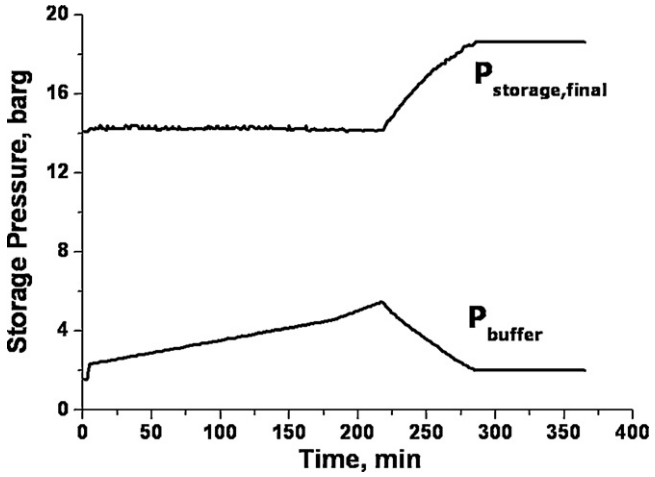

Fig. 11. Storage pressure during the PEM electrolyzer operation.

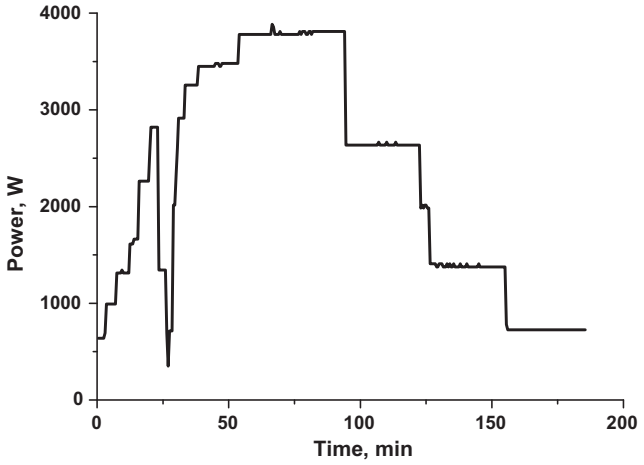

Fig. 12. Output power from the PEM fuel cell.

20% of its nominal power), which is considered as a normal case at the start-up operation time of this subsystem.

Fig. 11 shows the pressure in the hydrogen storage system, which is filled with hydrogen during the electrolyzer operation. The produced hydrogen is temporarily stored in the buffer tanks until the pressure inside these tanks reaches the limit of 5.5 barg. Then the compressor is used to further raise the pressure of hydrogen to the main storage tanks. An important issue in hydrogen storage systems is the constant monitoring on the buffer tanks pressure in order to avoid exceeding the maximum operating pressure limit.

A similar test experiment was also conducted for the analysis of the PEM fuel cell operation. As it can be seen from Fig. 12, the PEM fuel cell was tested for various levels of output power ranging from 0.6 kW to 3.8 kW which corresponds to a range of about 7 lt min^{-1} to 43 lt min^{-1} of hydrogen consumption, respectively. The storage pressure during the operation of the fuel cell is shown in Fig. 13, where its constant decrease due to the continuous hydrogen consumption can be observed. When the hydrogen inventory reaches the low operational pressure limit of 7 barg, the diesel generator is specified to be set to operation in order to provide power to the system instead of the fuel cell.

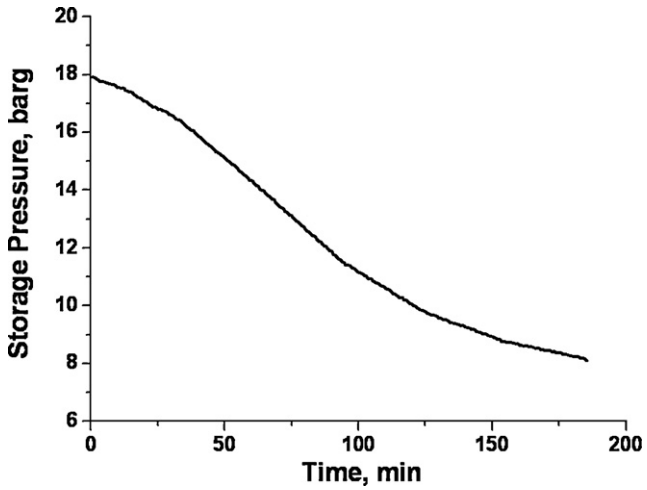

Fig. 13. Storage pressure during the PEM fuel cell operation.

5. One year simulation study

5.1. Description of the main power management strategy

In previous works [6,7], mathematical models for describing the subsystems (Fig. 1) operating feautures have been developed. Based on the analysis of various power management strategies [6,7], the operating strategy depicted in the flowchart of Fig. 5 was selected and for the present work is utilized and enhanced by including the diesel generator and compressor operation in the respective calculations. The main objective of the simulation study is to analyze and report the contribution of every subsystem in meeting three different constant load demands. Based on the simulation results, the subsystems which are affected more by this change of the load demand are identified and subsequently certain design modifications in the stand-alone power system could be proposed in order to apply an efficient operation without driving the subsystems to excessive use. Subsystems that operate less than expected could be down-scaled or even removed from the system, whereas others that contribute more than initially expected could be expanded in cases of a scale-up. Moreover, in order to minimize the environmental effect of the stand-alone power system, the diesel generator operation should be as minimal as possible. It is noted that the algorithm used in the simulation studies is the one presented in Fig. 5 where based on the calculation of power deficit or surplus and according to the *SOC* of the accumulator, certain decisions that dictate the operation of each subsystem are taken. Moreover, since the hydrogen storage system capacity is considered low for the real system a higher capacity value is used for the simulation studies. Fig. 14 presents the main details of the implemented power management strategy followed by an analysis on the various cases and on the importance of the hysteresis band zone as is included in Fig. 5.

The hysteresis band zone is defined as the acceptable band in the vicinity of minimum and maximum *SOC* limits that can allow:

- The accumulator to continue its operation (charging) beyond the maximum *SOC* limit (SOC_{max_charge}).
- The PEM electrolyzer to continue its operation by using power provided by the accumulator until SOC_{elec}.
- The PEM fuel cell to continue its operation until SOC_{fc}.

The introduction of the hysteresis band in the boundary limits of the *SOC* of the accumulator can also be seen in Fig. 5. This zone provides larger flexibility in the operation of the

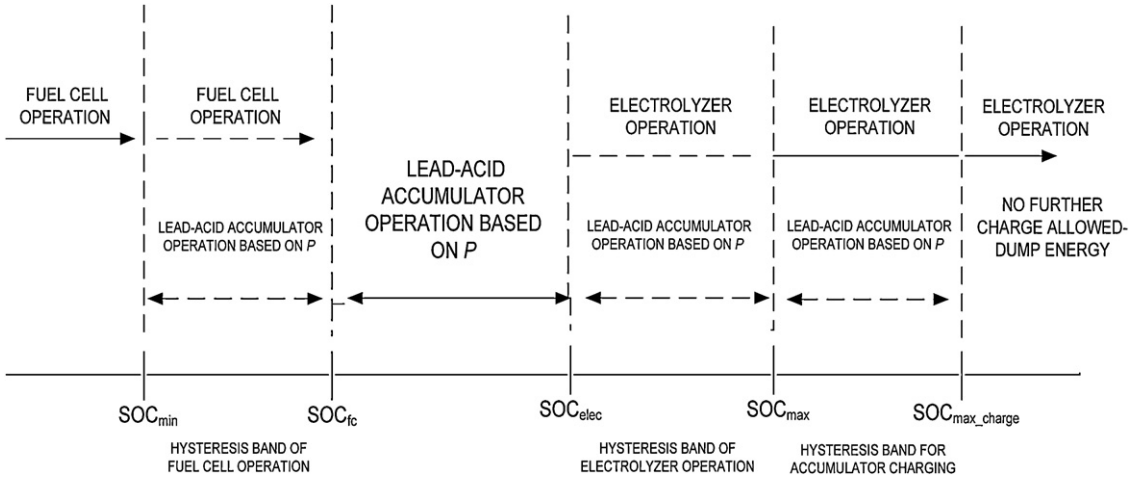

Fig. 14. Power management strategy for the stand-alone power system (- - -: operating according to *SOC* and power (*P*) values, —: always operating).

Table 1
Values of variables used in the simulation studies.

Hysteresis band zone limits (SOC_{nom} = 100% is the accumulator *SOC* when fully charged)	$SOC_{max\_charge} = SOC_{max} + 3\% \cdot SOC_{nom}$ $SOC_{fc} = SOC_{min} + 3\% \cdot SOC_{nom}$ $SOC_{elec} = SOC_{max} - 3\% \cdot SOC_{nom}$
SOC_{min}	80%
SOC_{max}	90%
$SOC_{initial}$	92%
Load	1–1.5–2 kW
Fuel cell output power	Equal to the load demand
Diesel generator output power	Equal to the load demand
Minimum operating power level of the electrolyzer, $P_{min,elec}$	1.05 kW
Maximum operating power level of the electrolyzer, $P_{max,elec}$	4.2 kW
Initial hydrogen inventory	200 N m^3 (about the 15% of the maximum capacity of the pressurized tanks equivalent to 300 kWh)
Initial storage pressure	7 barg
Maximum storage pressure	100 barg

electrolyzer, the fuel cell and the accumulator. In this way, the units can be protected from heavy and unnecessary utilization or irregular operation (reduction of frequent start-ups and shut-downs) [6]. Specifically, the addressed power management strategy facilitates the prolonged electrolyzer operation when conditions in the system impose the initiation of an electrolyzer operating session. It also maintains a smoother operation regardless of the instantaneous variations in the RES power production as long as $SOC > SOC_{elec}$. Similarly, the fuel cell follows a more efficient operating pattern with the use of the hysteresis band, as it is prevented from frequent start-ups and shut-downs in its operation when *SOC* is below or close to SOC_{min}. All decisions taken and implemented in the power management strategy are presented below and detailed information on the developed algorithm through logical block diagrams can be found in [7].

For $P \leq 0$ (*power deficit*)

(i) Case 1: ($SOC \leq SOC_{min}$): the accumulator is prevented from further discharging and the fuel cell is employed to provide the necessary power to meet the power deficit. In case the output power of the fuel cell is higher than the power deficit, this excess power is utilized to charge the accumulator. In case of a hydrogen deficit, the diesel generator operates in the place of the fuel cell as an emergency back-up unit.

(ii) Case 2: ($SOC_{min} < SOC < SOC_{fc}$): if the fuel cell is in operation, then it continues to operate until the *SOC* reaches the limit of SOC_{fc}. In case the fuel cell is not in operation or the hydrogen levels are below a critical level to support the fuel cell operation, then the accumulator discharges to satisfy the power deficit.

(iii) Case 3: ($SOC_{fc} \leq SOC$): The accumulator discharges to provide the power deficit to the system.

For $P > 0$ (*excess power*)

(i) Case 1: ($SOC_{max\_charge} < SOC$ and $P > P_{max,elec}$): the electrolyzer is utilized at its nominal power level and the excess power P-$P_{max,elec}$ is dumped.

(ii) Case 2: ($SOC_{max} < SOC < SOC_{max\_charge}$ and $P > P_{max,elec}$): the electrolyzer operates at a power equal to $P_{max,elec}$ and the excess power $P - P_{max,elec}$ is used to charge the accumulator without exceeding the SOC_{max_charge} limit.

(iii) Case 3: ($SOC_{max} < SOC$ and $P < P_{min,elec}$): the accumulator provides the power deficit of $P - P_{min,elec}$ in order to support the electrolyzer operation at its minimum power level.

(iv) Case 4: ($SOC_{max} < SOC$ and $P_{min,elec} \leq P \leq P_{max,elec}$): the RES fully and independently support the operation of the electrolyzer.

(v) Case 5: ($SOC_{elec} < SOC < SOC_{max}$): if the electrolyzer is in operation, it continues to operate, while the accumulator operates according to the cases 1–4.

(vi) Case 6: ($SOC \leq SOC_{elec}$): the lead-acid accumulator is charged by the available power from the RES.

In every sampling time period during the simulation (regardless of the power excess or shortage), the storage pressure of the buffer tanks is monitored. In case it exceeds the limit of 7 barg, the compressor starts to operate in order to fill the final storage tanks. The power demand of the compressor is provided solely by the accumulator. The values for the variables of Table 1 were used in the simulation studies.

Table 2
Average values per period for solar irradiation, air temperature and wind speed for each time period.

	January–April	May–August	September–December
G (W m^{-2})	119.6	224.8	103.8
T (°C)	10.6	25.3	17.6
v_{wind} (m s^{-1})	1.05	0.8	1.04

Table 3
Average (per period) net total energy (kWh) for each time period for three case studies of load demand.

Load demand	January–April	May–August	September–December	Overall
1 kW	5.13	34.2	−1.43	37.88
1.5 kW	−11.3	17.3	−18.14	−12.12
2 kW	−27.75	0.47	−34.84	−62.12

Table 4
Percentage of time (%) referring to the different *SOC* cases during the simulated period of one year for the three case studies of load demand.

Load demand	% time being at $SOC < SOC_{min}$	% time being at $SOC_{min} \leq SOC \leq SOC_{max}$	% time being at $SOC > SOC_{min}$	Sum
1 kW	11.78	68.21	20.01	100
1.5 kW	31.26	55.65	13.09	100
2 kW	44.73	45.83	9.44	100

5.2. Load demand variations

The simulation time step is selected to be 1 h which is suitable for representing the variation in the wind and solar energy for a one-year operation (8760 h). The employed mathematical models have been taken by [7] and are used in the present study. The input meteorological data during the given one year operation for the region of Neo Olvio, Xanthi have been collected and Table 2 presents the average values for the solar irradiation (G, W m^{-2}), air temperature (T, °C) and wind speed (v_{wind}, m s^{-1}) for each time period (four months).

Based on the system input data and according to the overall system mathematical model, the *PV*-array contribute 90.5% of the total produced power with the rest produced by the three wind generators system. To this end, the *PV*-array is considered as the main contributor to the power production in the system, since the regional wind speeds are too low for the wind generators to operate continuously.

Table 3 presents the average values of the net total energy, $E = E_{RES} - E_{LOAD}$ (similar as to Eq. (2) that referred to the net power), for the stand-alone power system in terms of energy excess (positive values) and energy shortage (negative values) for each time period of four months during a year of operation. As it can be seen, only during the summer period an energy excess is observed in the system for all cases of load demand, while during the remaining time of year a shortage of energy is observed, as the load demand is increased.

As it can be inferred, the increase in the energy deficit and the decrease in the energy excess as the load demand increases, is expected to be clearly depicted in the operation pattern of the accumulator and consequently, of the interconnected subsystems. The percentage of time (%) during the simulated year that represents the *SOC* operational behaviour is shown in Table 4. As it can be seen, the available time ($SOC > SOC_{max}$) for the electrolyzer operation is significantly reduced as load demand levels increase, with detrimental effects on hydrogen inventory. Also, the fuel cell consumes more and more hydrogen, due to the increase of time that *SOC* is below SOC_{min}. Fig. 15 depicts the hydrogen inventory during the one-year period of operation, which further explains the performance of the stand-alone power system based on the values of Tables 3 and 4.

Table 5
Total hydrogen production, consumption and average inventory over a one-year period for the three case studies of load demand.

Load demand	$H_{2,production}$, N m^3	$H_{2,consumption}$, N m^3	$H_{2,avg.inventory}$, N m^3
1 kW	684.8	497.1	328.8
1.5 kW	389.3	389.9	96.5
2 kW	250.5	250.1	73.1

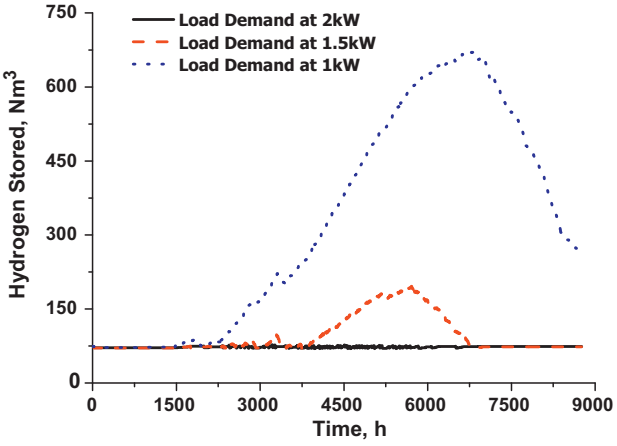

Fig. 15. Hydrogen inventory during the one-year period of operation for the three case studies of load demand.

In the case of the 1 kW load demand, there exists an increase in the hydrogen inventory, especially during the period May–August, where high renewable power production levels exist and the electrolyzer operates more frequently. During the remaining time of the year, due to the fact that a deficit of energy exists, the continuous fuel cell operation reduces the hydrogen inventory. Similar results are also recorded for the case of the 1.5 kW load demand, but with quite lower rates of increase during the respective period of May–August, whereas near the end of the year the hydrogen inventory is decreased up to its minimum operation levels. In the case of the 2 kW load demand the increase in the hydrogen inventory in the period of May–August is much lower (practically negligible) and the tanks contain hydrogen near the lower limit of 7 barg (equivalent to 74 N m^3) throughout the year. When the hydrogen inventory reaches the low limit of storage pressure in the tanks, the diesel generator operates for longer periods, a fact that leads to the excessive diesel consumption. Finally, Table 5 presents the values for the hydrogen production, consumption and average hydrogen inventory for the three case studies that further explains the trends that were observed in.

5.3. Analysis on the subsystems operation time and energy levels for the three case studies of load demand

Figs. 16 and 17 present the operation time and the corresponding energy levels in each subsystem for the three load demand case studies, respectively. As observed, the effect of an increase in the load demand causes a consequent decrease in the electrolyzer and fuel cell operation times and also to their energy levels, a result that was also expected by the *SOC* operation pattern described in Table 4 and the hydrogen production, consumption and storage values of Table 5. The compressor operation time and energy consumption are also decreased since the electrolyzer operates less frequently, going from the case of a load demand at 1 kW to that at 2 kW. In contrast, the diesel generator operates for longer periods of time, exhibiting quite high energy levels due to the low hydrogen inventory observed in the cases of a 1.5 and 2 kW load demand.

Table 6
Energy contribution in (kWh) and energy contribution percentage (%) of RES, accumulator, fuel cell and diesel generator at the various subsystems for the three case studies of load demands.

Load demand	Contributor to				
	Load	Accumulator	Electrolyzer	Compressor	Dump-loss
1 kW: RES at:	3730 (30.9)	4872.9 (40.4)	3280.8 (27.2)	–	194.4 (1.6)
1.5 kW: RES at:	5173.9 (42.8)	5036.1 (41.7)	1843.5 (15.3)	–	24.6 (0.2)
2 kW: RES at:	6434.4 (53.3)	4437.6 (36.7)	1200.8 (9.9)	–	5.3 (0.05)
1 kW: Accumulator at:	3938.7 (87.6)	–	118.3 (2.6)	437.4 (9.7)	–
1.5 kW: Accumulator at:	4548.9 (93.5)	–	88.8 (1.8)	235.4 (4.7)	–
2 kW: Accumulator at:	4368.7 (95.7)	–	42.6 (0.9)	153.7 (3.4)	–
1 kW: Fuel cell and diesel generator at:	1091.3 (86.2)	174.9 (13.8)	–	–	–
1.5 kW: Fuel cell and diesel generator at:	3417.2 (88.4)	450.1 (11.6)	–	–	–
2 kW: Fuel cell and diesel generator at:	6716.9 (90.6)	697.3 (9.4)	–	–	–

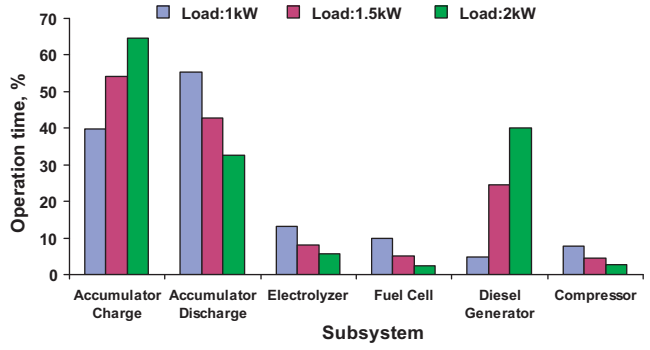

Fig. 16. Operation time of the various subsystems for the three case studies of load demand.

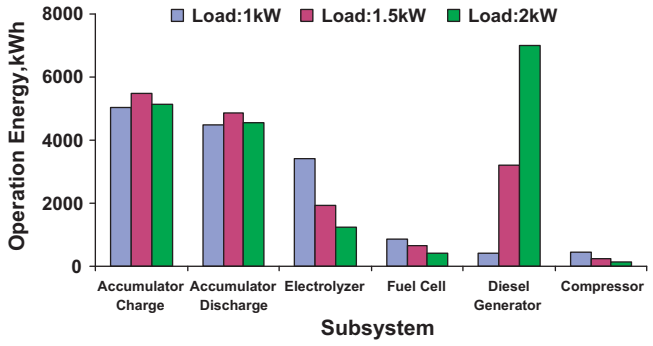

Fig. 17. Operation energy levels of the various subsystems for the three case studies of load demand.

Similarly, since the time period in which $SOC_{min} > SOC$ increases with an increase in the load demand, the charging time is increased, mainly due to the contribution of the diesel generator, whereas the decrease in the discharging time is attributed to the decrease in the available time for the electrolyzer operation ($SOC_{max} < SOC$). The energy levels however, for the respective cases of charging and discharging modes, do not follow the same pattern as the operation times of the accumulator which is a characteristic feature of the considered integrated system rather than a systematic observation. The cases of 1 kW and 2 kW load demands exhibit nearly similar energy levels, but higher levels are observed for the case of 1.5 kW, which is attributed to: (a) the increased energy supply of the combination of the RES, diesel generator and fuel cell to the accumulator (charging mode) and (b) to the increased energy supply of the accumulator to the load (discharging mode). In general, it is found that increasing the load demand beyond 1.5 kW always shows a decrease in the respective charging and discharging energy, while in the case of load demands below 1.5 kW, the charging and discharging energy levels depend heavily on the contribution to and from the various subsystems and on the overall net energy during the year (Table 3). If the net energy exhibits high negative levels then the accumulator charging and discharging energy are always lower.

One of the most detrimental effects of increasing the system load demand is the increase in the accumulator operating cycles that will eventually result in its early replacement. An operating cycle for the accumulator is defined as the process in which a discharging (or charging) mode is followed by a charging (or discharging) mode. Accumulator manufacturers provide semi-log diagrams that relate the total number of cycles that the accumulator can undergo in its lifetime period to the Depth-of-Discharge (DOD), the difference between $SOC_{max,charge}$ and SOC_{min} limits, [6,7]. For a given SOC_{min} and $SOC_{max,charge}$ levels, the % ratio of the operating cycles to the total allowable number of cycles for the accumulator can be determined and for the cases of 1 kW, 1.5 kW and 2 kW load demand these ratios were 16%, 19.3% and 21.8%, respectively. Lower values of this ratio indicate higher potential lifetime for the accumulator. The number of cycles is one of the most crucial parameters that should be taken into account as significant since higher operation and maintenance costs may arise. A value below 20%/year is usually suggested for stand-alone power systems [23]. It is noted though that the comparison of the real cycling of the accumulator with the simulated data that are presented in this analysis is not performed for the time being as it is scheduled for future studies. Instead an indirect evaluation of the battery cycling was used based on testing data performed by systems Sunlight (see Table A.1).

5.4. Analysis on the subsystems individual energy contribution for the three case studies of load demand

Table 6 presents the contribution of the RES, accumulator, fuel cell and diesel generator to the system energy needs for the three case studies, respectively. The main results are summarized below:

(a) *RES Supply*: as the load demand increases, the RES supply to meet the load demand is increased and the contribution to the electrolyzer operation is decreased. Based on the *SOC* values, the accumulator absorbs the remaining available energy from the RES to meet its electrical needs, while the surplus energy damping becomes lower for higher load demands.
(b) *Accumulator Supply*: as the load demand increases, the accumulator provides less power to the electrolyzer and consequently to hydrogen compression, since its main operation is for meeting the load demand (the energy percentage is higher as the load demand increases).
(c) *Fuel Cell and Diesel Generator Supply*: as the load demand increases, the total energy provided by the fuel cell and the

diesel generator to the load and to the accumulator increases, with the main characteristic result being the increase in the energy percentage for the load and the decrease for the accumulator.

Overall, it is concluded that the stand-alone power system presented is well designed to meet a 1 kW load demand, with sufficient hydrogen storage for fuel cell operation, while the conventional energy back-up diesel generator has limited operation. As the load demand is increased, the net energy throughout the year is observed to have a negative sign, which results in a lower hydrogen inventory accompanied by increased diesel consumption. Thus, in order to maintain a reliable system operation, with sufficient hydrogen stored and minimum diesel generator operation, an increase in the nominal installed capacity of the *PV*-array is suggested. The *PV*-system will support the electrolyzer operation for hydrogen production more frequently, which will be beneficial for the fuel cell operation, thus reducing in this way the activation of the diesel generator. Another modification could be the reduction in the SOC_{min} limit, which would prevent the frequent consumption of hydrogen in the fuel cell, but would simultaneously result in the reduction of the accumulator's lifetime, as it was found in previous studies [6]. It is noted that the case study analysis is based on a well-structured power management strategy [7] and on the operational experience gained from the stand-alone power system of Neo Olvio [23], which are both required in pre-design studies. For more in depth analysis, an optimal design study should describe the required modifications of the system by minimizing a predefined objective function [11,23]. The objective function should include the main design variables of concern, such as the subsystems nominal capacities or nominal operation levels that would be optimized, leading in this way to minimum operating and maintenance costs of the stand-alone power system.

6. Conclusions

In the present study, the control system and the automation architecture that is developed in a stand-alone power system at Neo Olvio in Greece were analyzed and evaluated. A proposed power management strategy was developed and implemented according to the accumulator *SOC* and the system net power calculations. As was shown for the real-time operation, the necessary step towards achieving reliability and autonomy in a RES-based system lies on the full understanding and hands-on experience from the involved subsystems along with their electronic parts that can eventually lead to the efficient operation under a central control unit. The proposed communication of the subsystems with the *SCADA* system enable remote users to monitor undergoing operations and perform changes in required system parameters and variables (flows, limits, etc.). Furthermore, the implemented operating control strategy was tested in simulation studies for a period of one-year, in order to draw important conclusions regarding complex decisions that could be used in future optimal design and operation studies of similar systems. The applied case scenarios involved the evaluation and analysis of the power system ability to compensate increased load demands, with ultimate aim the reliable, autonomous and eco-friendly operation. As it was found, an increase of 100% in the initial load demand, leads the diesel generator to high prolonged operating hours with a minimum hydrogen storage. In such a case, in order to fulfill the energy needs of the RES-power system, an increase of the *PV*-system installed capacity or a change in the limits of the *SOC* of the accumulator is suggested. However, the final decision should rely on optimal design studies that are currently under development.

Table A.1
Estimated number of cycles along with the respective DOD.

Depth of Discharge (%)	Number of cycles
80	1250
70	1429
60	1667
50	2000
40	2500
30	3333
25	4000
20	5000

Acknowledgements

The financial support of Greek General Secretariat for Research and Technology under the Ministry of Development is gratefully acknowledged. This study was conducted in the framework of the research project "AMΘ-9".

Appendix A. Operating cycling evaluations

A list of data referring to the expected cycle-life of the utilized accumulator (type OPzV) that is installed at the considered stand-alone power system of Neo Olvio, Xanthi are presented in Table A.1.[1]

The number of cycles (OPzV Expected Cycle-Life) as a function of DOD follows the general non-linear function based on the values of Table A.1:

$$\text{Number of cycles} = \frac{1000}{\text{DOD}} \quad \text{(A.1)}$$

The accumulator is allowed to operate at a DOD of 20–25% which is translated into a total of 4000–5000 cycles. The plan that is scheduled for the comparison involves the full operation of the integrated system under the proposed operation algorithm for more than 6 months continuously and the indirect estimation of the real cycling for this time period. According to the mathematical model a reliable comparison could be performed with high accuracy.

References

[1] P.A. Lehman, C.E. Chamberlin, G. Pauletto, M.A. Rocheleau, Int. J. Hydrogen Energy 22 (1997) 465–470.
[2] A. Brinner, H. Bussmann, W. Hug, W. Seeger, Int. J. Hydrogen Energy 17 (1992) 187–197.
[3] P.C. Ghosh, B. Emonts, H. Janßen, J. Mergel, D. Stolten, Sol. Energy 75 (2003) 469–478.
[4] A.M. Chaparro, J. Soler, M.J. Escudero, E.M.L. de Ceballos, U. Wittstadt, L. Daza, J. Power Sources 144 (2005) 165–169.
[5] P. Hollmuller, J.M. Joubert, B. Lachal, K. Yvon, Int. J. Hydrogen Energy 25 (2000) 97–109.
[6] D. Ipsakis, S. Voutetakis, P. Seferlis, F. Stergiopoulos, S. Papadopoulou, C. Elmasides, Energy 33 (2008) 1537–1550.
[7] D. Ipsakis, S. Voutetakis, P. Seferlis, F. Stergiopoulos, C. Elmasides, Int. J. Hydrogen Energy 34 (2009) 7081–7095.
[8] A. Nabil, M. Miyatake, A.K. Al-Othman, Energy Convers. Manage. 49 (2008) 2711–2719.
[9] S. Pedrazzi, G. Zini, P. Tartarini, Energy Convers. Manage. 51 (2010) 122–129.
[10] D.B. Nelson, M.H. Nehrir, C. Wang, Renew. Energy 31 (2006) 1641–1656.
[11] G. Giannakoudis, A.I. Papadopoulos, P. Seferlis, S. Voutetakis, Int. J. Hydrogen Energy 35 (2010) 872–891.
[12] S. Kélouwani, K. Agbossou, R. Chahine, J. Power Sources 140 (2005) 392–399.
[13] K. Zhou, J.A. Ferreira, S.W.H. De Haan, Int. J. Hydrogen Energy 32 (2008) 477–489.
[14] N. Forero, J. Hernández, G. Gordillo, Energy Convers. Manage. 47 (2006) 2329–2336.
[15] R. Akkaya, A.A. Kulaksiz, Appl. Energy 78 (2004) 419–431.
[16] C.M. Rangel, V.R. Fernandes, Y. Slavkov, L. Bozukov, J. Power Sources 181 (2008) 382–385.

[1] C. Elmasides, Data from cycling tests performed in Systems Sunlights's R&D Department, Unpublished Report, 2011.

[17] A. Bergen, L. Pitt, A. Rowe, P. Wild, N. Djilali, J. Power Sources 186 (2008) 158–166.
[18] A. Stefanopoulou, K.W. Suh, Control Eng. Pract. 15 (2007) 277–289.
[19] P. Roncero-Sánchez, V. Feliu-Batlle, A. García-Cerrada, Control Eng. Pract. 17 (2009) 255–266.
[20] K. Agbossou, M. Lal Kolhe, J. Hamelin, É. Bernier, T.K. Bose, Renew. Energy 29 (2000) 1305–1318.
[21] M. Little, M. Thomson, D. Infield, Int. J. Hydrogen Energy 32 (2007) 1582–1588.
[22] E. Koutroulis, K. Kalaitzakis, Renew. Energy 28 (2003) 139–152.
[23] S.S. Voutetakis, F. Stergiopoulos, P. Seferlis, S. Papadopoulou, D. Ipsakis, C. Ziogou, A.I. Papadopoulos, C. Elmasides, in: W.H. Lee, V.G. Cho (Eds.), Handbook of Sustainable Energy, Nova Publishers, 2010.
[24] S. Piller, M. Perrin, A. Jossen, J. Power Sources 96 (2001) 113–120.
[25] S. Lee, J. Kim, J. Lee, B.H. Cho, J. Power Sources 185 (2008) 1367–1373.
[26] S. Santhanagopalan, R.E. White, J. Power Sources 161 (2006) 1346–1355.
[27] T. Moor, J. Raisch, J.M. Davoren, Proceedings of IFAC Conference on Analysis and Design of Hybrid Systems, St. Malo, France, 2003, pp. 389–394.